Electrodeposition of Silicon Fibers from KI–KF–KCl–K$_2$SiF$_6$ Melt and Their Electrochemical Performance during Lithiation/Delithiation

Anastasia Leonova [1] , **Natalia Leonova** [1] , **Lyudmila Minchenko** [2] **and Andrey Suzdaltsev** [1,2,*]

1 Scientific Laboratory of Electrochemical Devices and Materials, Ural Federal University, Mira St. 19, 620075 Ekaterinburg, Russia; a.m.leonova@urfu.ru (A.L.); n.m.leonova@urfu.ru (N.L.)

2 Institute of High Temperature Electrochemistry UB RAS, Academicheskaya St. 20, 620066 Ekaterinburg, Russia; minchenko@ihte.ru

* Correspondence: a.v.suzdaltsev@urfu.ru

Abstract: The possibility of using Si-based anodes in lithium-ion batteries is actively investigated due to the increased lithium capacity of silicon. The paper reports the preparation of submicron silicon fibers on glassy carbon in the KI–KF–KCl–K$_2$SiF$_6$ melt at 720 °C. For this purpose, the parameters of silicon electrodeposition in the form of fibers were determined using cyclic voltammetry, and experimental samples of ordered silicon fibers with an average diameter from 0.1 to 0.3 μm were obtained under galvanostatic electrolysis conditions. Using the obtained silicon fibers, anode half-cells of a lithium-ion battery were fabricated, and its electrochemical performance under multiple lithiations and delithiations was studied. By means of voltametric studies, it is observed that charging and discharging the anode based on the obtained silicon fibers occurs at potentials from 0.2 to 0.05 V and from 0.2 to 0.5 V, respectively. A change in discharge capacity from 520 to 200 mAh g^{-1} during the first 50 charge/discharge cycles at a charge current of 0.1 C and a Coulombic efficiency of 98–100% was shown. The possibility of charging silicon-based anode samples at charging currents up to 2 C was also noted; the discharge capacity ranged from 25 to 250 mAh g^{-1}.

Keywords: silicon; electrodeposition; fibers; Si-anode; lithium-ion battery; electrochemical performance; capacity

1. Introduction

In order to increase the share of renewable energy utilization in the global energy industry, it is necessary to continuously improve materials and devices for energy conversion and storage [1]. One of these ways is to increase the energy density in lithium-ion batteries (LIBs). This can be achieved using anode materials with a capacitance exceeding that of graphite. Promising materials are silicon (discharge capacity up to 4200 mAh g^{-1}) [2,3], germanium (up to 1624 mAh g^{-1}) [4,5], transition metal oxides (up to 1200 mAh g^{-1}) [6,7], etc. Many of the above-mentioned materials cannot be used as an anode for a lithium-ion current source due to significant volume expansion (silicon—up to 300%, germanium and transition metal oxides—up to 100–200%, graphite—no more than 10%). So, various different compositions of the above materials with graphite are promising anode materials [8].

For silicon, high electrochemical performance in lithiation and delithiation can be also ensured using nanosized and submicron particles or thin films [9]. The advantage of silicon thin films and fibers over micro- and macro-crystalline silicon particles may lie in their probable amorphous nature or lack of any long-range atomic ordering [10]. This has been reported in many papers dealing with the fabrication and testing of thin-film silicon anodes. Amorphousness in this case does not depend on whether they were synthesized using physical or chemical methods. As a rule, amorphous materials are predominantly

characterized by better performance (stability of discharge capacitance, lower value of irreversible capacitance loss) compared to their crystalline counterparts. For example, in [11], a nanostructured silicon anode was synthesized as a thin film with nanocrystalline particles with an average diameter of ~12 nm and as a continuous thin film with a thickness of ~100 nm. The amorphous silicon thin-film anode showed an initial discharge capacity of ~3500 mAh g^{-1} and retained the capacity up to ~2000 mAh g^{-1} for 50 cycles, while the nanocrystalline silicon showed a discharge capacity of approximately 1100 mAh g^{-1} with only ~50% capacity retention after 50 cycles. This behavior of thin films was explained using their amorphous structure [12]. Some decrease in capacitance was explained by the fact that during lithiation, phase transformations occur in the anode sample with the formation of Li_5Si_4 silicide, which is only partially consumed during delithiation, which also leads to the peeling of the silicon film from the substrate [13]. Although the results obtained indicate high silicon performance and relative stability, they are limited and require further optimization. The same conclusion was reached in our previous work, where a discharge capacity of 715 mAh g^{-1} after 10 cycles was observed for electrodeposited silicon fibers [14].

Traditionally, obtaining silicon of specified sizes involves a number of operations: reduction of quartz to silicon of metallurgical purity; chlorination and hydrochlorination of metallurgical silicon; reduction of chlorosilanes to silicon crystals; zone recrystallization of silicon; and obtaining silicon-based anodes using plasma or laser sputtering methods [15]. Methods for the electrolytic deposition of silicon of a given morphology from molten salts are an alternative [1,16–18].

One of the most promising and frequently used electrolytes for silicon production are water-soluble KF–KCl melts with K_2SiF_6, SiO_2, and $SiCl_4$ additives [19–21]. Nowadays, the kinetics of the cathodic process depending on the substrate material and polarization conditions has been well studied, experimental samples of silicon deposits depending on the electrolysis parameters have been obtained, and a diagram characterizing the influence of these parameters on the morphology of silicon deposits has been proposed [21]. The regulation of silicon deposits' morphology can also be realized by introducing additives into the electrolyte that influence the physicochemical properties of the electrolyte and the parameters of electrochemical nucleation. This is primarily concerned with changing the electrical conductivity and surface tension of the melt. Earlier [22], it was proposed that we could use halide melts based on iodides for this purpose. As a result of previous studies, the possibility of obtaining thin silicon films and their microalloying was shown [23].

The present work shows the possibility of using KI-KF-KCl-K_2SiF_6 melt for electrodeposition of submicron silicon fibers for their application in the anode of a lithium-ion battery.

2. Experiment

For electrochemical measurements and electrodeposition, we used chemically pure salts (JSC "Vekton", St.Petersburg, Russia), which were preliminarily purified from impurities using hydrofluorination (KF, K_2SiF_6) and iodination (KI), as well as preliminary potentiostatic electrolysis [20,22]. Silicon electrodeposition was carried out in a sealed stainless-steel retort [20] filled with electrochemically purified argon. The container for the melt was a glassy carbon crucible placed in a graphite container. A graphite cylinder was used as the working electrode, while monocrystalline silicon served as the counter electrode and quasi-reference electrode. The retort was placed in a vertical resistance furnace and heated to the operating temperature of 720 °C. The electrodeposition parameters were determined on the basis of voltammograms, which were recorded on a glassy carbon electrode using the same setup. The melt temperature was set using an *S*-type thermocouple and a USB-TC01 thermocouple module (National Instruments, Austin, TX, USA). At the end of electrolysis, the deposits were washed from the electrolyte residue in aqueous HF solution and dried in a vacuum at 200 °C.

The morphology and elemental composition of the obtained samples were investigated using a Tescan Vega 4 scanning electron microscope (Tescan, Brno, Czech Republic) with an Xplore 30 EDS detector (Oxford, UK).

The electrochemical performance of the obtained silicon fibers was investigated in a three-electrode half-cell [24]. An electrically conductive additive of 10 wt% graphite and 10 wt% binder (CMC in deionized water) was used in order to fabricate a Si-based anode. The anode half-cells of LIBs were fabricated as follows. The anode mass (total mass of 0.002 g) of the above composition was placed onto the current lead (made of stainless-steel mesh) and dried under a vacuum for 24 h at 110 °C. Then, the prepared anode was brought into a sealed glove box filled with argon (O_2, H_2O < 0.1 ppm), where the half-cell under study was fabricated. For this purpose, the working electrode, counter electrode, and reference electrode (both made of lithium foil) were placed in a fluoroplastic cell. All electrodes were divided using two layers of separator (propylene). After that, the cell was filled with electrolyte 1 M $LiPF_6$ in an EC/DMC/DEC mixture (1:1:1 by volume). All electrolyte reagents were of 99.99% purity (Sigma-Aldrich, St. Louis, MI, USA). Voltammetric measurements and experiments of multiple lithiation/delithiation with different currents were performed using PGSTAT P-20X8 (Electrochemical Instruments, Chernogolovka, Russia).

3. Results and Discussion

Voltammetry in KI–KF–KCl–K_2SiF_6 melt. To determine the parameters (potential, current density) of silicon electrodeposition on glassy carbon in KI–KF–KCl–K_2SiF_6 melt voltammetry dependence was obtained, which is shown in Figure 1. The investigated process starts at potentials negative to 0 V relative to the silicon quasi-reference electrode with the formation of a single cathodic peak of electroreduction in silicon ions at a potential of about −0.17 V and a cathodic current density of 0.08 A cm^{-2}. Further shifting of the glassy carbon potential leads to potassium release and electrode destruction. When sweeping the working electrode potential into the anodic region, a single dissolution peak of electrodeposited silicon is also formed at a potential of 0.12 V and an anodic current density of 0.10 A cm^{-2}.
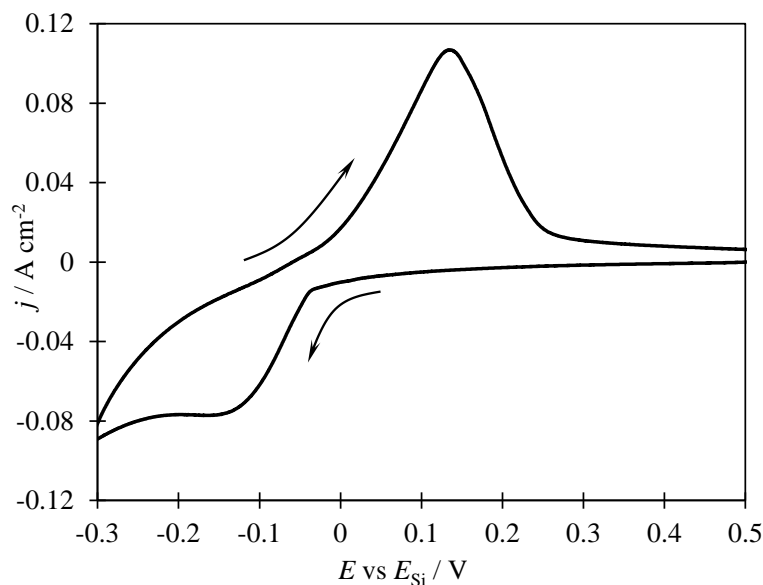

Figure 1. Typical voltametric dependence obtained on glassy carbon in (mol%) 75KI–16KF–8KCl–1K$_2$SiF$_6$ melt at temperature 720 °C and potential sweep rate 0.02 V s^{-1}.

The form of the voltametric dependence indicates the occurrence of the investigated process in one four-electron stage under the experimental conditions. Similar dependences were obtained in halide melts of other compositions [3,19–23]. Based on electrochemical measurements, a cathodic current density of 0.05 A cm^{-2} was chosen for the electrodeposition of silicon in the form of particles with a high specific surface area.

Morphology of the obtained silicon. The electrodeposition of silicon from KI–KF–KCl–K_2SiF_6 melt on glassy carbon was carried out at a cathodic current density of 0.05 A cm^{-2}. The cathode potential ranged from -0.1 to -0.2 V relative to the potential of the silicon quasi-reference electrode. SEM-images of the obtained silicon after washing in HF solution are shown in Figure 2. The obtained silicon deposits were represented using orderly shaped fibers with average diameters from 0.1 to 0.3 µm and lengths from 5 to 20 µm. This morphology provides a high specific surface area for lithium intercalation. EDS analysis shows 99.2–99.8 wt% silicon in obtained samples with expected oxygen residual impurities.
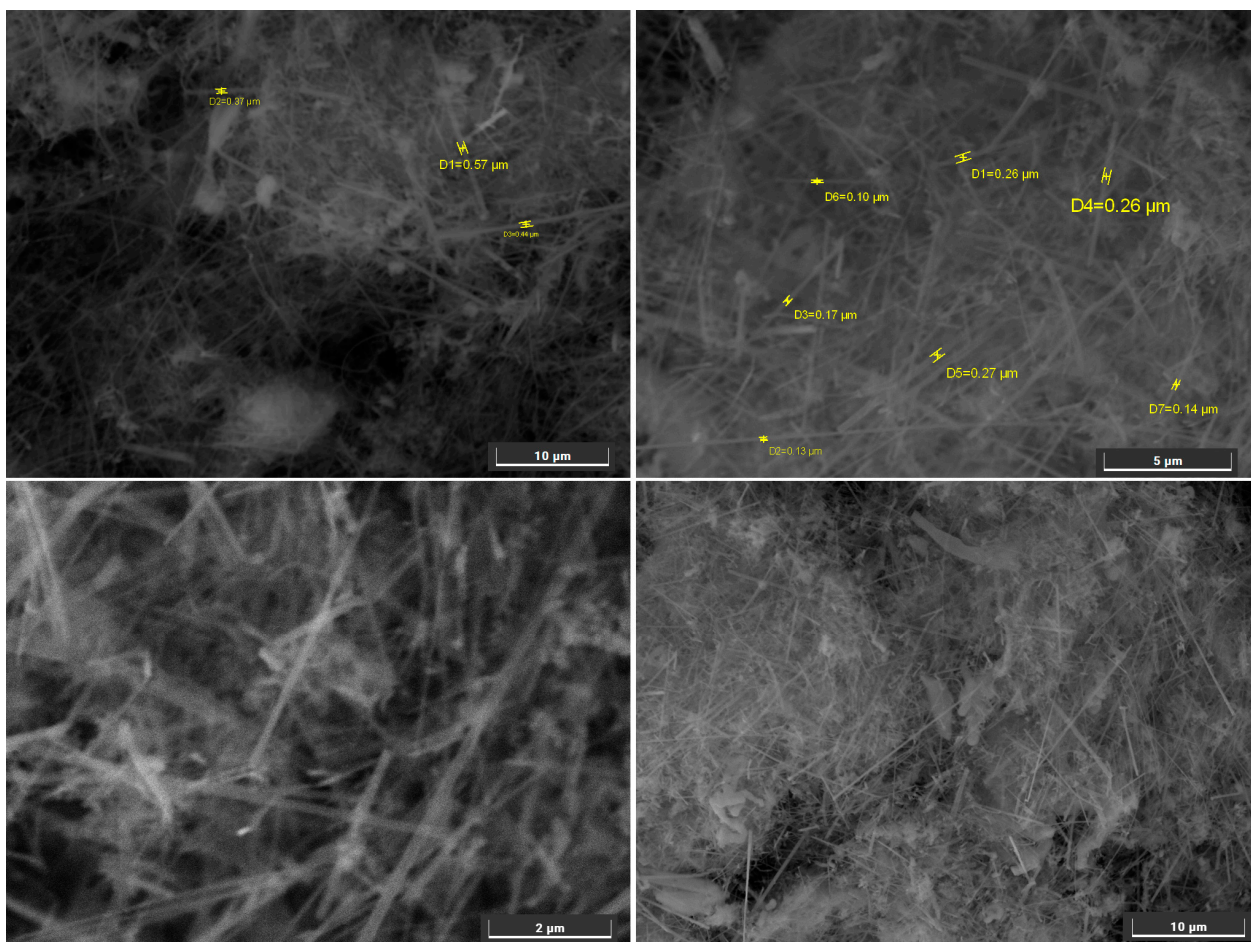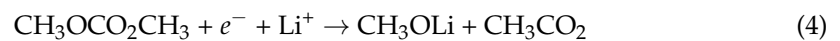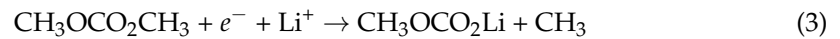

Figure 2. SEM-images of silicon deposits obtained using electrolysis of KI–KF–KCl–K_2SiF_6 melt on glassy carbon at cathodic current density of 0.05 A cm^{-2} and temperature 720 °C for 60 min.

Electrochemical performance. Figure 3a shows the cyclic voltametric dependences for the initial six charge–discharge cycles. The first two lithiation/delithiation cycles are significantly different from the post-lithiation cycles, with Coulomb efficiencies of 65 and 78% for the first and second cycles, respectively. Such values of efficiency for the first cycles are typical for the majority of investigated silicon-based anodes [1–3]. According to many sources, a significant value of irreversible capacity at the first two cycles is associated with side reactions between electrolyte components (reactions (1)–(14)), formation of an interfacial lithium-conducting layer at the electrode–electrolyte interface (SEI), and irreversible reactions using reduced lithium and residual SiO_2 (reactions (15) and (16)) [24–26]. In the case of the electrolyte we used, the reactions are listed below:
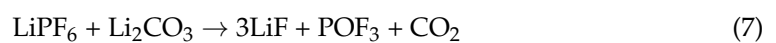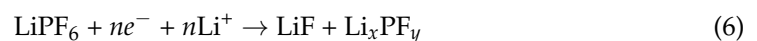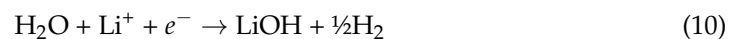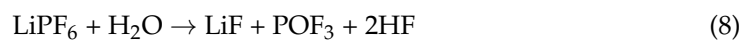
for EC

$$(CH_2O)_2CO + 2e^- + 2Li^+ \rightarrow Li_2CO_3 + C_2H_4 \tag{1}$$

$$2(CH_2O)_2CO + 2e^- + 2Li^+ \rightarrow (CH_2OCO_2Li)_2 + C_2H_4 \tag{2}$$

for DMC

$$CH_3OCO_2CH_3 + e^- + Li^+ \rightarrow CH_3OCO_2Li + CH_3 \tag{3}$$

$$CH_3OCO_2CH_3 + e^- + Li^+ \rightarrow CH_3OLi + CH_3CO_2 \tag{4}$$

for $LiPF_6$

$$LiPF_6 \rightarrow LiF + PF_5 \tag{5}$$

$$LiPF_6 + ne^- + nLi^+ \rightarrow LiF + Li_xPF_y \tag{6}$$

$$LiPF_6 + Li_2CO_3 \rightarrow 3LiF + POF_3 + CO_2 \tag{7}$$

for H_2O

$$LiPF_6 + H_2O \rightarrow LiF + POF_3 + 2HF \tag{8}$$

$$H_2O + Li^+ + e^- \rightarrow Li_2O + H_2 \tag{9}$$

$$H_2O + Li^+ + e^- \rightarrow LiOH + \tfrac{1}{2}H_2 \tag{10}$$

$$ROCO_2Li + H_2O \rightarrow Li_2CO_3 \tag{11}$$

for HF

$$Li_2CO_3 + HF \rightarrow LiF + H_2O + CO_2 \tag{12}$$

$$ROCO_2Li + HF \rightarrow LiF + ROCO_2H \tag{13}$$

$$Li_2O + HF \rightarrow LiF + H_2O \tag{14}$$

for SiO_2

$$2SiO_2 + 4Li^+ + 4e^- \rightarrow Li_4SiO_4 + Si \tag{15}$$

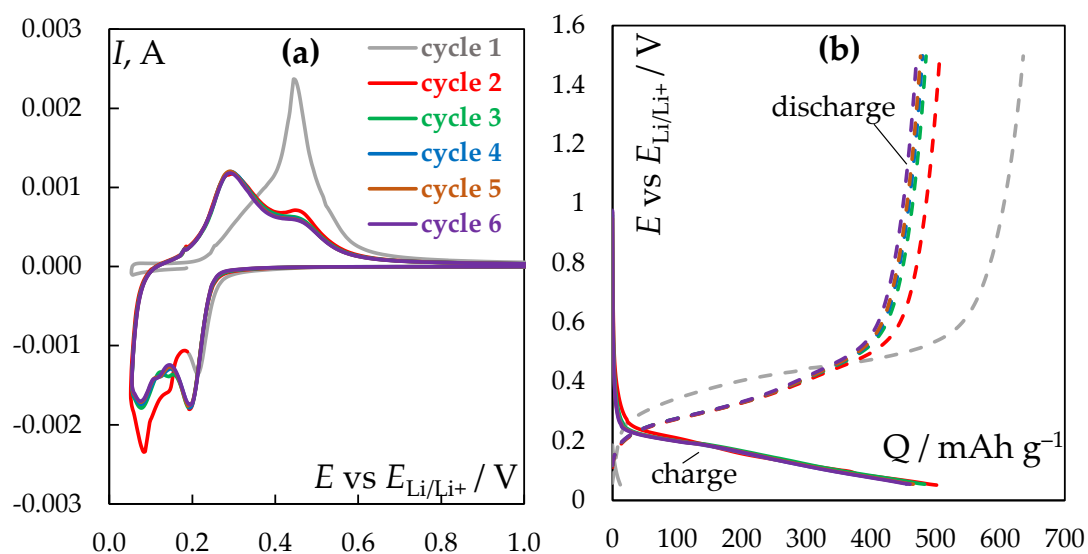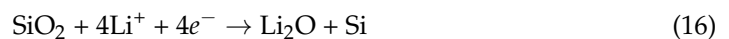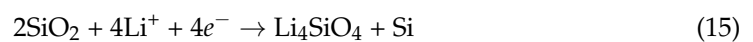$$SiO_2 + 4Li^+ + 4e^- \rightarrow Li_2O + Si \tag{16}$$
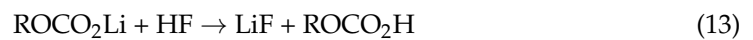
Figure 3. Cyclic voltammetry (**a**) and charge–discharge dependencies (**b**) characterizing the behavior of the silicon fiber-based anode during the initial 6 lithiation/delithiation cycles.

In addition to increased energy costs, a significant value of irreversible capacitance leads to irreversible loss of part of the lithium ions, both in the electrolyte and in the cathode material. A decrease in the amount of available lithium in the composition of the cathode can lead to its mechanical destruction and a decrease in the conductivity of the electrolyte and electrical insulation of the areas where poorly conductive Li_4SiO_4 and Li_2O are formed. This will adversely affect the long-term operation of the lithium-ion battery. Its formation usually occurs in the first one–two cycles, after which voltametric dependences begin to reproduce [14,27].

By the third cycle, the reproducibility of the obtained dependences is observed. In the cathodic region, one can note peaks in the potential region negative to 0.2 V associated with the discharge of lithium ions and the formation of Li_xSi_y-type compounds of variable composition via reactions, i.e.,

$$Si + xLi+ + xe \rightleftarrows Li_xSi \tag{17}$$

$$Li_xSi + yLi+ + ye \rightleftarrows Li_{(x+y)}Si \tag{18}$$
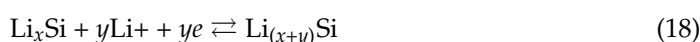
To prevent the release of elemental lithium, the sweep was carried out to a potential of 0.05 V relative to the potential of the lithium electrode. In the anodic region, two distinct peaks were formed at potentials around 0.3 and 0.48 V, associated with the oxidation of lithium from the obtained Li_xSi_y compounds. Figure 3b shows the charge–discharge dependencies corresponding to the initial six cycles in potential-capacity coordinates. According to the given data, the charge proceeds in the potential region from 0.2 to 0.05 V, while the discharge proceeds at a potential from 0.2 to 0.5 V. This indicates the capacitive character of the lithium reduction reaction with its subsequent intercalation into the silicon volume.

The dependences in Figure 4 characterize the electrochemical behavior of the anode based on the obtained silicon fibers under multiple lithiation with a 0.1 C current (Figure 4a) as well as with different currents (Figure 4b). During the first 50 cycles, the discharge capacity decreased from 520 to 200 mAh g^{-1}, after which it stabilized at the value of 200–220 mAh g^{-1}. Figure 4b shows the possibility of charging the studied samples at high currents up to 2 C. Also, despite the relatively low values of the discharge capacity, the operability of the fabricated anode half-cell during a relatively high number of cycles is noted. At current C, the fabricated anode was cycled for 600 cycles. The discharge capacity at the first cycle was 41, and at the last cycle it was 9 mAh g^{-1}, indicating a gradual degradation of this material.
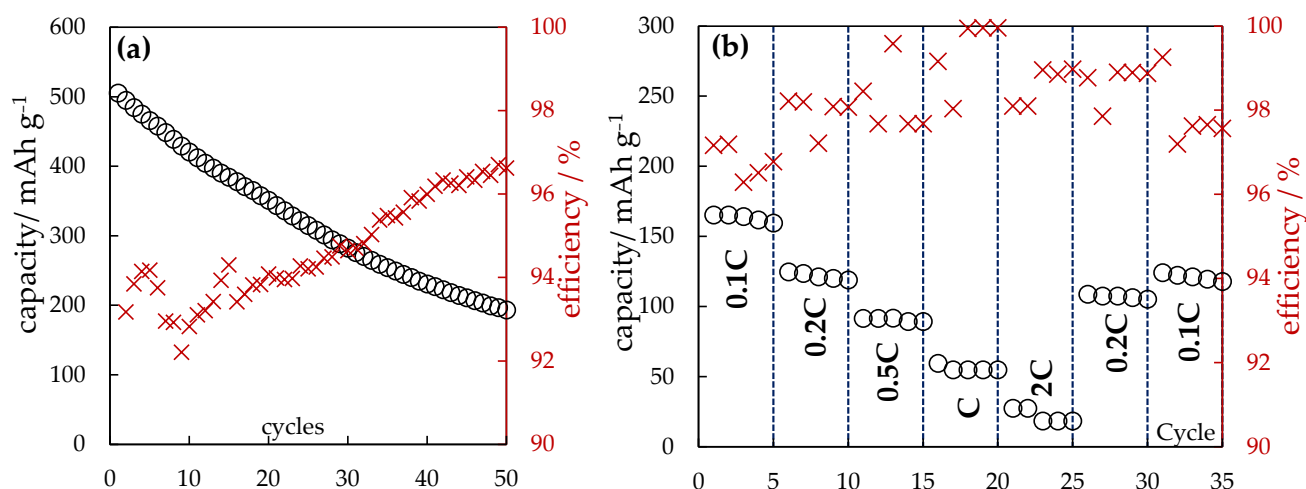

Figure 4. Variation of discharge capacity and Coulombic efficiency of silicon fiber-based anode at multiple lithiation/delithiation with 0.1 C current (**a**) and different charge currents (**b**).

The results obtained are comparable to the results of studies on the electrochemical behavior of electrodeposited silicon fibers from other melts [3,14,22], while the relatively low capacitance and its decrease during cycling may indicate degradation of the liquid electrolyte or the substrate–anode interface. Therefore, the behavior of the obtained silicon fibers should be studied with other electrolytes and structural materials. In particular, many works studied both the performance of silicon anodes with solid and polymer electrolytes [28–30] and the performance of mixtures of silicon of different morphologies with graphite [31,32], oxides [33,34], carbides, and other materials [35].

4. Conclusions

The cathodic process on glassy carbon in the (mol%) $75KI–16KF–8KCl–1K_2SiF_6$ melt at 720 °C has been studied using cyclic voltammetry. It is shown that the investigated process proceeds in one stage: silicon electroreduction takes place in the potential range from 0 to -0.3 V relative to the potential of the silicon quasi-reference electrode. On the basis of electrochemical measurements, the parameters of silicon electrodeposition in the form of deposits with a high specific surface area were chosen: cathodic current density of 0.05 A cm^{-2} with control of the cathode potential. During galvanostatic electrolysis of the $KI–KF–KCl–K_2SiF_6$ melt, silicon particles in the form of ordered-shaped fibers with an average diameter from 0.1 to 0.3 μm and length from 5 to 20 μm were obtained.

The obtained silicon fibers were used to fabricate a sample of the anode half-cell of LIB in order to study the electrochemical behavior of the obtained silicon during lithiation/delithiation. It is shown that the charge of the anode based on the obtained silicon fibers takes place at potentials from 0.2 to 0.05 V relative to the lithium potential, which is due to the formation of lithium–silicon compounds. Accordingly, the anode discharge occurs at potentials from 0.2 to 0.5 V. A change in discharge capacity from 520 to 200 mAh g^{-1} during the first 50 charge/discharge cycles at a charge current of 0.1 C and a Coulombic efficiency of 98–100% is shown. The possibility of charging silicon-based anode samples at charging currents up to 2 C was also noted; the discharge capacity was 25 to 250 mAh g^{-1}.

It is concluded that it is necessary to conduct further studies using alternative materials of electrolyte and current supply to the anode.

Author Contributions: Conceptualization, A.S.; methodology; L.M., A.L. and N.L.; validation, L.M., A.L. and N.L.; formal analysis, L.M., A.L. and N.L.; investigation, L.M., A.L. and N.L.; writing—original draft preparation, A.L. and A.S.; writing—review and editing, A.S.; supervision, A.S.; project administration, A.S. All authors have read and agreed to the published version of the manuscript.

Institutional Review Board Statement: Not applicable.

Informed Consent Statement: Not applicable.

Data Availability Statement: Data are contained within the article.

Conflicts of Interest: The authors declares no conflicts of interest.

References

1. Miao, J. Review on Electrode Degradation at Fast Charging of Li-Ion and Li Metal Batteries from a Kinetic Perspective. *Electrochem* **2023**, *4*, 156–180. [CrossRef]
2. Wang, F.; Li, P.; Li, W.; Wang, D. Electrochemical Synthesis of Multidimensional Nanostructured Silicon as a Negative Electrode Material for Lithium-Ion Battery. *ACS Nano* **2022**, *16*, 7689–7700. [CrossRef] [PubMed]
3. Wan, Y.; Yang, W.; Jin, C.; Shi, B.; Xu, G.; Yue, Z.; Li, Y.; Sun, F.; Zhou, L. Preparation of Porous Silicon by Ag-assisted Chemical Etching in Non-Filling Type Carbon Shell for High Performance Lithium-Ion Batteries. *Solid State Sci.* **2023**, *145*, 107329. [CrossRef]
4. Stokes, K.; Flynn, G.; Geaney, H.; Bree, G.; Ryan, K.M. Axial Si–Ge Heterostructure Nanowires as Lithium-Ion Battery Anodes. *Nano Lett.* **2018**, *18*, 5569–5575. [CrossRef] [PubMed]

5. Kulova, T.L. New Electrode Materials for Lithium-Ion Batteries (Review). *Rus. J. Electrochem.* **2013**, *49*, 1–25. [CrossRef]

6. Hata, M.; Tanaka, T.; Kato, D.; Kim, J.; Yonezawa, S. Preparation of LiNiO$_2$ Using Fluorine-modified NiO and Its Charge-discharge Properties. *Electrochemistry* **2021**, *89*, 223–229. [CrossRef]

7. Purwanto, A.; Muzayanha, S.U.; Yudha, C.S.; Widiyandari, H.; Jumari, A.; Dyartanti, E.R.; Nizam, M.; Putra, M.I. High Performance of Salt-Modified–LTO Anode in LiFePO$_4$ Battery. *Appl. Sci.* **2020**, *10*, 7135. [CrossRef]

8. Saddique, J.; Wu, M.; Ali, W.; Xu, X.; Jiang, Z.-G.; Tong, L.; Zheng, H.; Hu, W. Opportunities and Challenges of Nano Si/C Composites in Lithium Ion Battery: A Mini Review. *J. Alloys Comp.* **2024**, *978*, 173507. [CrossRef]

9. Galashev, A.Y. Molecular Dynamic Study of the Applicability of Silicene Lithium Ion Battery Anodes: A Review. *Electrochem. Mat. Techn.* **2023**, *2*, 20232012. [CrossRef]

10. Li, P.; Hwang, J.; Sun, Y. Nano/microstructured Silicon–Graphite Composite Anode for High-energy-density Li-Ion Battery. *ACS Nano* **2019**, *13*, 2624–2633. [CrossRef] [PubMed]

11. Salah, M.; Hall, C.; Murphy, P.; Francis, C.; Kerr, R.; Stoehr, B.; Rudd, S.; Fabretto, M. Doped and Reactive Silicon Thin Film Anodes for Lithium Ion Batteries: A review. *J. Power Sources* **2021**, *506*, 230194. [CrossRef]

12. Graetz, J.; Ahn, C.C.; Yazami, R.; Fultz, B. Highly Reversible Lithium Storage in Nanostructured Silicon. *Electrochem. Solid-State Lett.* **2003**, *6*, A194–A197. [CrossRef]

13. Iaboni, D.S.M.; Obrovac, M.N. Li$_{15}$Si$_4$ Formation in Silicon Thin Film Negative Electrodes. *J. Electrochem. Soc.* **2016**, *163*, A255–A261. [CrossRef]

14. Trofimov, A.A.; Leonova, A.M.; Leonova, N.M.; Gevel, T.A. Electrodeposition of Silicon from Molten KCl–K$_2$SiF$_6$ for Lithium-Ion Batteries. *J. Electrochem. Soc.* **2022**, *169*, 020537. [CrossRef]

15. Prosini, P.P.; Rufoloni, A.; Rondino, F.; Santoni, A. Silicon Nanowires Used as the Anode of a Lithium-Ion Battery. *AIP Conf. Proc.* **2015**, *1667*, 020008. [CrossRef]

16. Padamata, S.K.; Saevarsdottir, G. Silicon Electrowinning by Molten Salts Electrolysis. *Front. Chem.* **2023**, *11*, 1133990. [CrossRef]

17. Dong, Y.; Slade, T.; Stolt, M.J.; Li, L.; Girard, S.N.; Mai, L.; Jin, S. Low-Temperature Molten-Salt Production of Silicon Nanowires by the Electrochemical Reduction of CaSiO$_3$. *Angew. Chem.* **2017**, *129*, 14645–14649. [CrossRef]

18. Pavlenko, O.B.; Ustinova, Y.A.; Zhuk, S.I.; Suzdaltsev, A.V.; Zaikov, Y.P. Silicon Electrodeposition from Low-Melting LiCl–KCl–CsCl Melts. *Rus. Met.* **2022**, *2022*, 818–824. [CrossRef]

19. Zaykov, Y.P.; Zhuk, S.I.; Isakov, A.V.; Grishenkova, O.V.; Isaev, V.A. Electrochemical Nucleation and Growth of Silicon in the KF–KCl–K$_2$SiF$_6$ Melt. *J. Solid State Electrochem.* **2015**, *19*, 1341–1345. [CrossRef]

20. Kuznetsova, S.V.; Dolmatov, V.S.; Kuznetsov, S.A. Voltammetric Study of Electroreduction of Silicon Complexes in a Chloride–Fluoride Melt. *Russ. J. Electrochem.* **2009**, *45*, 742–748. [CrossRef]

21. Yasuda, K.; Kato, T.; Norikawa, Y.; Nohira, T. Silicon Electrodeposition in a Water-Soluble KF–KCl Molten Salt: Properties of Si Films on Graphite Substrates. *J. Electrochem. Soc.* **2021**, *168*, 112502. [CrossRef]

22. Abdurakhimova, R.K.; Laptev, M.V.; Leonova, N.M.; Leonova, A.M.; Schmygalev, A.S.; Suzdaltsev, A.V. Electroreduction of Silicon from the NaI–KI–K$_2$SiF$_6$ Melt for Lithium-Ion Power Sources. *Chim. Techno Acta* **2022**, *9*, 20229424. [CrossRef]

23. Laptev, M.V.; Khudorozhkova, A.O.; Isakov, A.V.; Grishenkova, O.V.; Zhuk, S.I.; Zaikov, Y.P. Electrodeposition of Aluminum-Doped Thin Silicon Films from a KF–KCl–KI–K$_2$SiF$_6$–AlF$_3$ Melt. *J. Serb. Chem. Soc.* **2021**, *86*, 1075–1087. [CrossRef]

24. Zhao, X.; Lehto, V.-P. Challenges and Prospects of Nanosized Silicon Anodes in Lithium-Ion Batteries. *Nanotechnology* **2021**, *32*, 042002. [CrossRef]

25. Guo, J.; Dong, D.; Wang, J.; Liu, D.; Yu, X.; Zheng, Y.; Wen, Z.; Lei, W.; Deng, Y.; Wang, J.; et al. Silicon-Based Lithium Ion Battery Systems: State-of-the-art from Half and Full Cell Viewpoint. *Adv. Funct. Mater.* **2021**, *31*, 2102546. [CrossRef]

26. Mu, T.; Lou, S.; Holmes, N.G.; Wang, C.; He, M.; Shen, B.; Lin, X.; Zuo, P.; Ma, Y.; Li, R.; et al. Reversible Silicon Anodes with Long Cycles by Multifunctional Volumetric Buffer Layers. *ACS Appl. Mater. Interfaces* **2021**, *13*, 4093–4101. [CrossRef]

27. Veith, G.M.; Doucet, M.; Sacci, R.L.; Vacaliuc, B.; Baldwin, J.K.; Browning, J.F. Determination of the Solid Electrolyte Interphase Structure Grown on a Silicon Electrode Using a Fluoroethylene Carbonate Additive. *Sci. Rep.* **2017**, *7*, 6326. [CrossRef]

28. Liu, X.; Wang, D.; Wang, X.; Wang, D.; Li, Y.; Fu, J.; Zhang, R.; Liu, Z.; Zhou, Y.; Wen, G. Designing Compatible Ceramic/Polymer Composite Solid-State Electrolyte for Stable Silicon Nanosheet Anodes. *Small* **2024**, *in press*. [CrossRef]

29. Gu, L.; Han, J.; Chen, M.; Zhou, W.; Wang, X.; Xu, M.; Lin, H.; Liu, H.; Chen, H.; Chen, J.; et al. Enabling Robust Structural and Interfacial Stability of Micron-Si Anode Toward High-Performance Liquid and Solid-State Lithium-Ion Batteries. *Energy Storage Mat.* **2022**, *52*, 547–561. [CrossRef]

30. Na, I.; Kim, H.; Kunze, S.; Nam, C.; Jo, S.; Choi, H.; Oh, S.; Choi, E.; Song, Y.B.; Jung, Y.S.; et al. Monolithic 100% Silicon Wafer Anode for All-Solid-State Batteries Achieving High Areal Capacity at Room Temperature. *ACS Energy Lett.* **2023**, *8*, 1936–1943. [CrossRef]

31. Hossain, H.M.; Chowdhury, M.A.; Hossain, N.; Md. Islam, A.; Md. Mobarak, H.; Hasan, M.; Khan, J. Advances on Synthesis and Performance of Li-Ion Anode Batteries-a Review. *Chem. Eng. J. Adv.* **2024**, *17*, 100588. [CrossRef]

32. Yudha, C.S.; Sari, E.P.; Dewi, D.K.; Paramitha, T.; Suci, W.G. Utilization of Coal Fly-Ash derived Silicon (Si) as Capacity Enhancer of Li-Ion Batteries Anode Material. *E3S Web Conf.* **2024**, *481*, 01007. [CrossRef]

33. Kuang, H.; Xiao, L.; Lai, Y.; Shen, L.; Zhou, A.; Wu, J.; Zhu, Y. Effect of Si Doping and Active Carbon Surface Modifications on the Structure and Electrical Performance of Li$_4$Ti$_5$O$_{12}$ Anode Material for Lithium-Ion Batteries. *Ionics* **2024**, *in press*. [CrossRef]

34. Sun, B.; Wang, S.; Zhou, S.; Liu, J.; Mao, C.; Liu, K.; Fan, H.; Xie, J.; Song, J. Biomimetics-Inspired Architecture Enables the Strength–Toughness of Ultrahigh-Loading Silicon Electrode. *Adv. Funct. Mater.* 2024, *in press*. [CrossRef]

35. Kumaran, B.; Bhairuba Ikhe, A.; Pyo, M. Silicon Nanoparticles Encapsulated in Si_3N_4/Carbon Sheaths as an Anode Material for Lithium-Ion Batteries. *Nanotechnology* **2023**, *34*, 255401. [CrossRef]